AAS 13-420

ASSESSMENT OF THE MARS SCIENCE LABORATORY ENTRY, DESCENT, AND LANDING SIMULATION

David W. Way*, Jody L. Davis†, and Jeremy D. Shidner‡

On August 5, 2012, the Mars Science Laboratory rover, Curiosity, successfully landed inside Gale Crater. This landing was only the seventh successful landing and fourth rover to be delivered to Mars. Weighing nearly one metric ton, Curiosity is the largest and most complex rover ever sent to investigate another planet. Safely landing such a large payload required an innovative Entry, Descent, and Landing system, which included the first guided entry at Mars, the largest supersonic parachute ever flown at Mars, and a novel and untested Sky Crane landing system. A complete, end-to-end, six degree-of-freedom, multi-body computer simulation of the Mars Science Laboratory Entry, Descent, and Landing sequence was developed at the NASA Langley Research Center. In-flight data gathered during the successful landing is compared to pre-flight statistical distributions, predicted by the simulation. These comparisons provide insight into both the accuracy of the simulation and the overall performance of the vehicle.

INTRODUCTION

On August 5, 2012, at 10:32 PDT*, the Mars Science Laboratory (MSL) *Curiosity* rover successfully landed on Mars. After completing a 252 day, 568x10^6 km, inter-planetary transit, *Curiosity* entered the Martian atmosphere 125 km above the surface and traveling at 5.845 km/s. During the next seven minutes, the rover flawlessly executed a complex sequence of autonomous actions, safely coming to rest just 2.385 km away from the 4.5965 ^oS and 137.4019 ^oE target inside Gale Crater. These seven minutes were an extremely critical and challenging phase of the MSL mission, known as Entry, Descent, and Landing (EDL). At nearly 900 kg, a full five times heavier than the previous *Spirit* and *Opportunity* rovers, *Curiosity* is the largest and most sophisticated rover to ever explore beyond Earth.

The challenges associated with landing a rover that is the size of a small car, coupled with unprecedented requirements for accuracy, led to the development of a unique EDL system architecture that incorporates both heritage and innovation, while extending the limits of the Viking-derived EDL technologies qualified by the Mars Viking, Mars Pathfinder (MPF), and Mars Exploration Rover (MER) missions.[3] Accordingly, several elements of the MSL EDL design were technological firsts for Mars, such as the first guided entry and the novel "Sky Crane" landing system. These elements, now flight-validated, form an important step forward for the future of Mars exploration, which will likely require the precise landing of even larger payloads.

Because of differences in atmosphere and gravity, end-to-end EDL system verification and validation tests are not possible on Earth. Mars flight projects must, therefore, rely heavily on computer simulation results. Consequently, the EDL simulation is a key element in any successful landing. Simulation predictions are used throughout the project lifecycle: to inform EDL design choices, to compare and certify candidate landing sites, to verify EDL system performance, to select flight software parameters, and to evaluate operational decisions. Considering the importance of these activities, it is crucial for the EDL simulation to accurately,

*National Aeronautics and Space Administration, Langley Research Center, MS 489, Hampton, VA 23681-2199.
†National Aeronautics and Space Administration, Langley Research Center, MS 489, Hampton, VA 23681-2199.
‡Analytical Mechanics Association, Inc., 303 Butler Farm Road Suite 104A, Hampton, VA 23666.
*Earth Received Time.

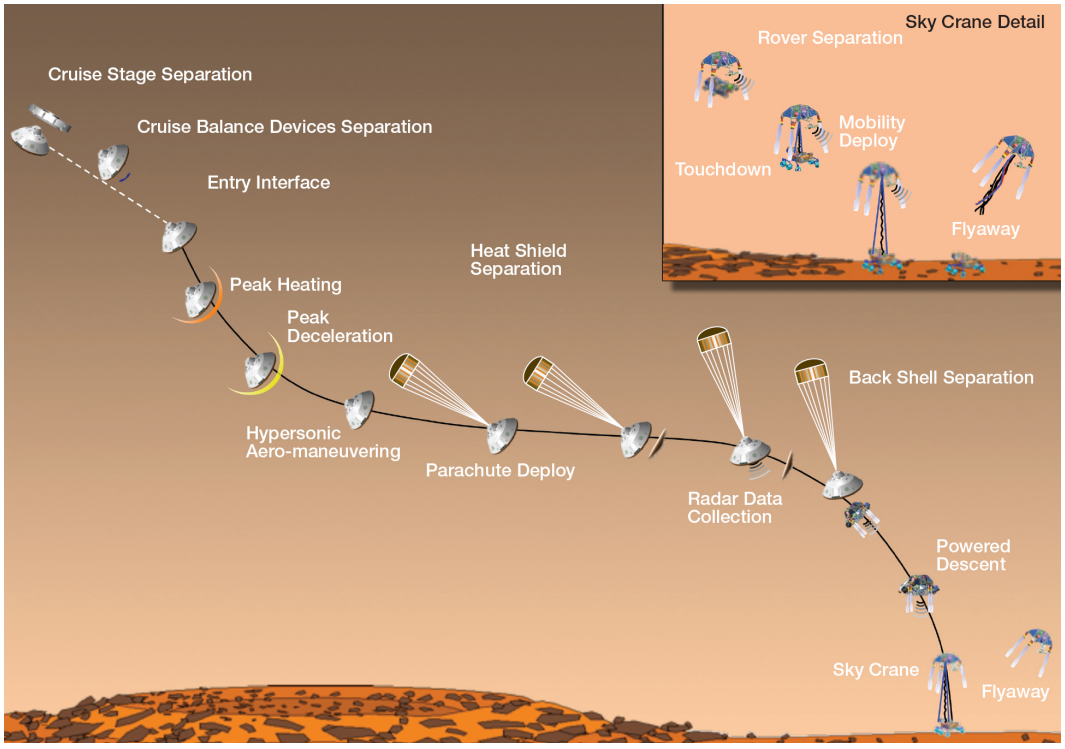

Figure 1: MSL EDL event sequence, Cruise Stage Separation to Flyaway. Image Credit: NASA/JPL-Caltech.

yet conservatively, model and predict the complex flight dynamics of the EDL system. Since each successful mission leads progressively forward in succession to the next, it is vitally important to the EDL community for each mission to provide a critical assessment of the EDL simulation and the models used. This assessment is made by comparing data collected in-flight, along with post-flight reconstructions, to pre-entry simulation predictions. This paper provides an assessment of the MSL EDL simulation.

MSL POST2 SIMULATION

The Program to Optimize Simulated Trajectories II (POST2) is a general Six Degree-of-Freedom (6-DoF) trajectory simulation tool, that solves both the translational and rotational equations of motions for up to 20 independent rigid bodies. It is maintained by the NASA Langley Research Center and has been used to solve a wide variety of flight dynamics and trajectory optimization problems. More germanely however, POST2 has had significant Mars EDL flight heritage. POST2 has been used successfully on the Mars Pathfinder,[4] Mars Exploration Rover (MER),[5] Mars Phoenix[6],[8] and now Mars Science Laboratory (MSL) missions.

A complete, end-to-end, POST2 simulation of Curiosity's complex EDL sequence was developed at the NASA Langley Research Center. This simulation was designated as the prime EDL performance simulation for MSL. Reference[3] contains a detailed description of the MSL EDL architecture, which is illustrated here in Figure 1. This architecture consists of six segments: Exo-atmospheric Flight, Guided Entry, Parachute Descent, Powered Descent, Sky Crane, and Flyaway. Reference[?] provides a description of the sensed triggers used at critical transitions.

The POST2 simulation modeled all events of the MSL EDL sequence, beginning 50 s after Cruise Stage separation. Arguably one of the largest and most complex simulations of its kind, it leveraged the versatility and heritage of previous POST2 simulations and added MSL-specific models and flight software. Fourteen independent bodies were modeled, including the Descent Stage, the parachute, the heatshield, the backshell,

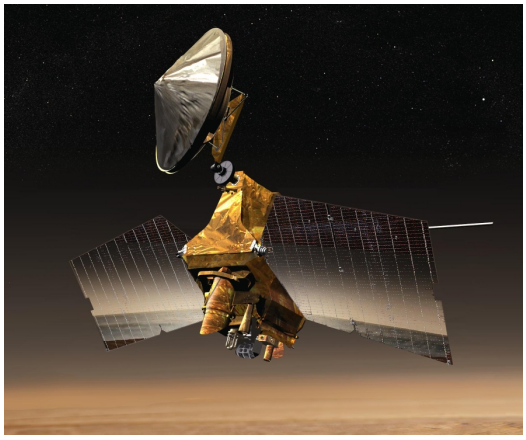

Figure 2: Artist's concept of the Mars Reconnaissance Orbiter (MRO). Image Credit: NASA/JPL-Caltech.

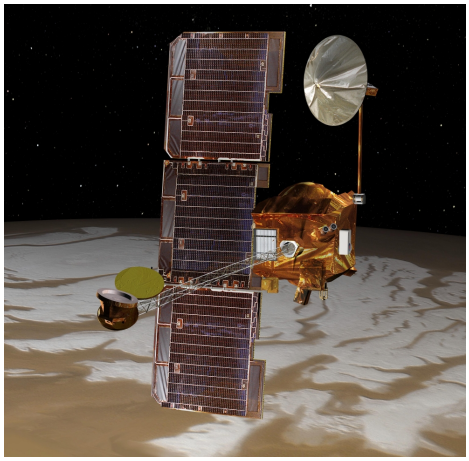

Figure 3: Artist's concept of the 2001 Mars Odyssey (ODY). Image Credit: NASA/JPL-Caltech.

the rover, and each of the eight ejected balance masses. Multi-body forces, originally developed for MER, were also used to model vehicle configurations containing two or more of these elements during two of the EDL segments. The first of these was the Parachute Descent segment, in which the parachute and backshell were attached via parachute riser lines. The second was the novel Sky Crane segment, in which the Descent Stage and rover were attached via the Bridle, Umbilical, and Descent Rate Limiter (BUD).

The EDL simulation is used to assess the robustness of the EDL system to off-nominal or uncertain conditions by tracking statistics on pre-defined output variables. These output variables are typically instantaneous flight conditions at specific events (e.g. Mach number at parachute deploy), but may also be minima or maxima of flight parameters experienced over specific regions or segments of EDL sequence (e.g. maximum entry deceleration). These outputs are collected, in a Monte Carlo fashion, over thousands of individual instantiations of the simulation, where each case contains random samples of uncertain parameters, such as initial states and environmental variables. The MSL simulation contained 682 random dispersions and 4834 output variables.

Purpose

The purpose of this paper is to compare reconstructed flight parameters to pre-flight simulation predictions in-order to evaluate the effectiveness of the simulation in modeling the flight. The as-flown values are compared to statistical distributions predicted by the simulation. Table 1, compiled from multiple sources, summarizes these comparisons. In each case, the Gaussian quantile of the as-flown value is measured, relative to the Monte Carlo results. This measurement is expressed as a number of standard deviations (e.g. 3σ). Values within approximately +/-1.5σ indicate good agreement, while values outside of +/-3σ indicate a significant disagreement between actual and simulated results.

Initial information available from real-time data products received via telemetry indicated that the MSL EDL sequence proceeded very nominally, culminating in a landing just 2.385 km downrange of the intended target. All Timeline Engine timepoints occurred within 6.9089 s of their predicted mean times. However, further analysis has uncovered three anomalies (and several intentional conservatisms) where performance varied from simulation predictions. These anomalies are discussed in the following sections.

TELECOMMUNICATIONS

Throughout EDL, UHF transmissions from *Curiosity* were monitored by three Mars orbiters: the Mars Reconnaissance Orbiter (Figure 2), 2001 Mars Odyssey (Figure 3), and European Space Agencys Mars Express.

A geometry-based EDL communications model was added to POST2 to assist in the EDL communications analysis. This model utilized SPICE ephemeris kernels (containing the orbiter trajectories), C-Matrix kernels (containing attitude information), and antenna gain patterns, and the terrain model of the landing region to determine expected UHF acquisition and loss times.

Monte Carlo analysis of link closure to MRO indicated that the 1 to 99 %-tile times of acquisition occurred between $E-$08:20 (Entry minus 8 minutes and 20 seconds) and $E-$07:36. In flight, the MRO link was established at $E-$08:07, indicating a 1.494σ event. The loss of link was expected to be occur between $E+$12:50 and $E+$13:03 for the 1 and 99 percentile results respectively. The loss of link to MRO occurred at $E+$13:08, indicating a 3.557σ event. The improved link performance for MRO could be attributed either to discrepancies in the horizon mask analysis or trajectory differences between the predicted MRO location and actual location.

The link closure analysis to ODY indicated an acquisition of signal at $E+$02:44 and $E+$02:47 at the 1 and 99 percentile results respectively. The short separation in time is due to using the OD230 initial states which caused the 8,000 Monte Carlo samples to have their first bank reversal occur nearly coincident in time. The first bank reversal in turn causes the PUHF antenna pattern to be better directed to ODY, increasing the total received power to the lock threshold. In flight, the ODY link was established at $E+$03:42 seconds after entry interface, indicating a 3.836σ event. The discrepancy is due to the POST2 simulation not modeling RF behavior such as carrier pulses, plasma blackout, and transmitter-off periods.[19] The loss of link was expected to occur between $E+$12:29 and $E+$15:10 at the 1 and 99 percentile results respectively. In flight, the signal was lost at $E+$13:07, indicating a -0.973σ event. The early loss of signal relative to the 0 sigma point is likely due to landing 2.4 km long, which would have caused ODY to set earlier due to the horizon masking of Mt. Sharp.

EXO-ATMOSPHERIC FLIGHT

Cruise Stage Separation (CSS) occurred at $E-$10:00. At $E-$09:00, referred to as TZERO ($t = 0s$), the EDL GN&C was activated.

Following a period of Reaction Control System (RCS) warm-up, the Entry Vehicle (EV) is de-spun from the constant 2 rpm spin rate used through-out Cruise and then re-oriented to the desired entry attitude. Two Cruise Balance Masses (CBMs) were jettisoned at 50.640625 and 51.140625 s, providing the center-of-mass offset required to generate an L/D of 0.24 at Mach 24.

The Entry Controller then maintained this attitude, within dead-bands, through atmospheric Entry Interface (EI) until the Range Control phase of the Entry Guidance begins.

During this exo-atmospheric phase, peak Entry Controller attitude and rate errors were nominal. Water-marks on these control errors are presented in Table 1. The largest quantile, calculated relative to the OD229 Monte Carlo predictions, was 1.509σ.

ENTRY

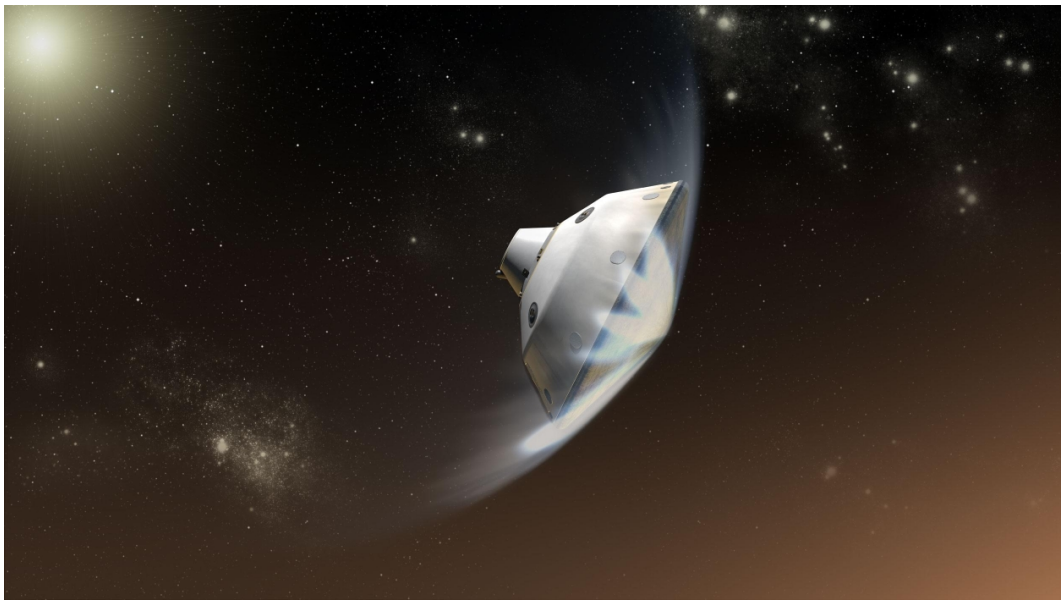

Figure 4: Artist's concept of the MSL spacecraft entering the Martian atmosphere during the Entry, Descent and Landing of the *Curiosity* rover. Image Credit: NASA/JPL-Caltech.

The Entry segment of EDL is the first of three major steps in slowing the spacecraft from its hypersonic entry speed 5.845 km/s. During this segment 99.6% of the Entry Vehicle's kinetic energy was removed through friction with the atmosphere. During this time, the spacecraft experienced nearly 13 $Earth\ g's$ of deceleration, while performing the first ever guided entry at Mars. The Entry segment consisted of four sub-phases: Wait For Guidance Start, Range Control, Heading Alignment, and SUFR. Each of these is discussed below.

WAIT FOR GUIDANCE START

By definition, atmospheric Entry Interface (EI) occurred 540.0 s following TZERO, at a geocentric radius of 3522.02 km. The vehicle entered the Martian atmosphere at a planet-relative velocity of 5845.4 m/s and an Entry Flight Path Angle (EFPA) of -15.474 deg, 631.979 km down-range of and 7.869 km cross-range of the landing target. At this point the Entry Controller was maintaining the programmed pre-bank angle of 80.3 deg while the GN&C Mode Commander transitioned to Mode 8, "WAIT FOR GUIDANCE START". The observed time in this mode was 45.875 s, which is -3.836σ and less than the 46.0 s minimum time predicted by the simulation. This was the first anomaly where actual conditions varied significantly from pre-flight predictions.

Mode 8 was active from EI to the start of active range control, which was a sensed trigger of 0.2 $Earth\ g's$ of deceleration. Thus, the duration of Mode 8 depends on the deceleration experienced at very high altitudes. The extremely short time spent in this mode is indicative of much higher than expected deceleration in the upper atmosphere (above 50 km). This could be explained by either a higher atmospheric density in this region and/or a higher drag coefficient. While it is not, in general, possible to separate the effects of drag coefficient and atmospheric density, it is estimated that their product would need to have been approximately 20% higher than nominal to produce the observed deceleration.

The net result of the quick deceleration through Mode 8 was to initiate Range Control early, at a 1.761 km higher altitude (3.836σ) and 7.8 km further from the target (numsig3.836) than the expected mean. This initialized the entry guidance in a condition that was significantly different than the reference trajectory.

The entry guidance responded to this situation by commanding an initial bank angle that was more lift-up than the pre-bank by 8.595 deg. In order to prevent large control errors, the initial guidance command was profiled, which was the purpose of GN&C Mode 9, "RANGE CONTROL SLEW TO COMMANDED BANK ANGLE". The observed time in Mode 9, which is proportional to the size of the profiled turn, was 2.51σ. Therefore, the long time in Mode 9 was also consistent with, and a direct result of, the high deceleration experienced prior to Range Conrol (above 58 km altitude).

Whatever the cause for the higher deceleration during Mode 8 (density or drag), the situation quickly corrected itself. By the time the vehicle completed Mode 9, the deceleration had returned to within 10% of the nominal value and the entry guidance began converging the range. Consequently, there were no lasting effects on entry performance, which is not surprising given the capability of the guidance to adjust to off-nominal conditions and the small fraction of the total deceleration that occurs above 50 km. Due to the minor impact on the rest of the entry, this anomaly is interesting, but not of concern for future missions. However, additional work may be warranted to better understand entry vehicle aerodynamics in this regime and to reconcile differences between the atmosphere models and observed temperature measurements at these high altitudes. In addition, alternate trigger algorithms may be less sensitive to uncertainties in deceleration, resulting in better matching of expected reference trajectory conditions.

RANGE CONTROL

As discussed in the previous section, Range Control began early at the following conditions: $t = 585.875\ s$, $V = 5863.599\ m/s$, $h_{MSL} = 58.600\ km$, $R_{down} = 378.350\ km$, and $R_{cross} = 7.773\ km$. During the Range Control phase, the bank angle was commanded to minimize predicted downrange error at parachute deploy. Throughout this phase, cross-range error was managed by executing three bank reversals, which occurred at $t = 612.875\ s$, $t = 633.875\ s$, and $t = 663.375\ s$. Peak heating and peak deceleration also occurred during this guidance phase. The "Atmospheric Entry" section of Table 1 presents several entry watermarks: peak entry deceleration (-0.471σ), peak entry lateral loads (1.060σ), and peak aerothermodynamic pressure (-1.658σ). Additional aerothermodynamic quantities (such as peak heatrate and total heatload) are not yet available, since final reconstruction of these quantities is still in progress.[?]

Aerodynamic performance during this phase has been reconstructed by Schoenenberger et al.[20] This reconstruction shows extremely good agreement between the model and flight data above the MEDLI operating range of 850 Pa (approximately Mach 3). The trim angle of attack was predicted accurately and the reconstructed lift-to-drag ratio exceeded predictions by only a small percentage for most of entry. Schoenenberger et al. also note that there was very little RCS activity during this phase, indicating that Aero-RCS interactions were benign. Likewise, control errors during this phase indicate that the Entry Controller performed nominally and encountered a low disturbance environment.[14]

HEADING ALIGNMENT

At a navigated velocity of 1100 m/s, the entry guidance transitioned to heading alignment in-order to minimize cross-range error prior to parachute deploy. Flight conditions at this time where: $t = 675.625\ s$, $R_{down} = 83.238\ km$, and $R_{cross} = 2.946\ km$. At this point, the vehicle was flying nearly full-lift-up and no longer controlling range-to-go. Because the range is open-loop, the vehicle is now susceptible to range errors due to atmospheric or aerodynamic dispersions. The overall time in Heading Alignment was slightly long at numsig1.135. Independently, this would not be of concern and it indicates good agreement with the simulation. However, as discussed in the next section, the time in SUFR was 3.200σ long. This indicates, therefore, that the anomalous supersonic deceleration experienced during SUFR likely began during heading alignment, prior to SUFR start.

Throughout both Range Control and Heading Alignment, peak Entry Controller attitude and rate errors were nominal. Watermarks on these control errors are presented in Table 1. The largest quantile during these two phases, calculated relative to the OD229 Monte Carlo predictions, was 0.920σ.

SUFR

Just prior to parachute deploy, the vehicle trim angle-of-attack was reduced to near zero by ejecting six Entry Balance Mass Devices (EBMDs) at two second intervals, in a maneuver referred to as Straighten-Up and Fly Right (SUFR). During this time a 180 deg roll is also commanded to place the TDS beams in a configuration more favorable for acquiring the ground. Flight conditions at this time were: $t = 779.875\ s$, $R_{down} = 12.817\ km$, and $R_{cross} = 0.527\ km$. The length of the SUFR maneuver was nominally targeted to be 17 s, to allow sufficient time to eject the masses and complete the roll. However, both SUFR start and parachute deploy were triggered by navigated velocities, which allowed this time to vary with the supersonic aerodynamic deceleration experienced between approximately Mach 2 to Mach 1.7.

Throughout the SUFR maneuver, the GN&C Mode Commander operates in two successive GN&C modes: Mode 14, "SLEW AND SUFR SLEW TO RADAR ATTITUDE"; and Mode 15, "SLEW AND SUFR WAIT FOR CHUTE DEPLOY". The observed time in these two GN&C modes was 14.0 s and 5.25 s, respectively, with a combined time between SUFR and PD of 19.25 s. This represents a 3.200σ event, relative to the simulation predictions, and indicates very low supersonic deceleration. Additionally, semi-independent reconstructions disagree on the value of aerodynamic angles (α and β) at SUFR start.[20] These off-nominal trim angles may also have contributed to slightly larger control errors during this phase, since the attitude dead-bands were tripped during the bank acceleration portion of the SUFR slew, causing the actual bank angle to fall behind the profile.[14] Watermarks on these control errors are presented in Table 1. The largest quantile, calculated relative to the OD229 Monte Carlo predictions, was 2.787σ.

Low deceleration in this flight regime could be indicative of several condtions: a high ballistic coefficient (due to a low drag coefficient); a low atmospheric density; or a tail wind (which depresses the dynamic pressure). While all of these conditions are both possible and difficult to differentiate, it appears likely that a modest tail wind was more likely the culprit. Karlgaard et al. estimated a tail wind of approximately 20 m/s using a Kalman filter reconstruction approach.[?]

Though the low supersonic deceleration likely contributed to landing downrange of the target, the extra 2.25 s spent waiting for parachute deploy had very little additional impact on the rest of the EDL system. During this time it is estimated that the vehicle decelerated approximately 5.6 m/s, traveled approximately 840 m downrange, and lost approximately 340 m of altitude. This altitude loss was of little consequence due the ample altitude margin available at Gale crater. However, future missions may consider replacing the parachute deploy trigger with a timed trigger, effectively making the parachute mortar fire a part of the SUFR timepoint sequence, and removing any possibility of trigger collisions. Even so, additional investigation into this anomaly is warranted to better understand the expected aerodynamic performance in this critical flight regime.

PARACHUTE DEPLOY

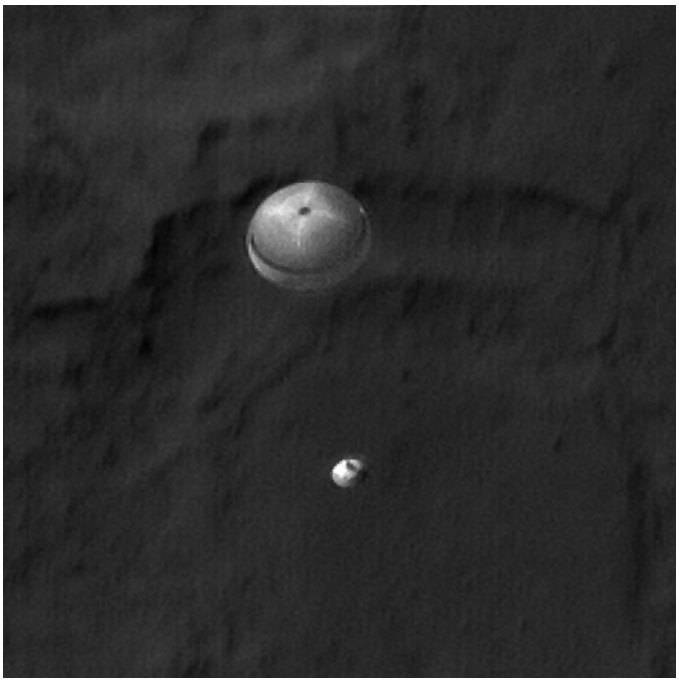

Figure 5: The High-Resolution Imaging Science Experiment (HiRISE) camera captured this image of *Curiosity* descending on parachute. Image Credit: NASA/JPL-Caltech/Univ. of Arizona

Parachute deploy occurred at $t = 799.125\ s$, $R_{down} = 4.964\ km$, and $R_{cross} = 0.318\ km$. Additional parachute deploy conditions were reconstructed, as described in Cruz et al.,[7] using the MMM5 meso-scale atmosphere model. This model was adjusted post-flight to match surface pressure measurements collected by REMS. The reconstructed conditions at parachute deploy were very nominal: Mach number (0.749σ), dynamic pressure (-0.019σ), altitude (0.144σ), and flight path angle (-1.345σ). The reconstructed instantaneous angle-of-attack (3.52^o), though high in terms of quantiles at 2.341σ, was 1^o less than the predicted 99%-tile and significantly below the 12^o limit.

Cruz et al. estimated the peak opening load of the parachute to be 34,580 lb_f, which is significantly below the 65,000 lb_f rating. This value is compared in Table 1 to two simulation calculations. The first of these calculations, F_{peak}, which is based on the drag coefficient modeled in the simulation, slightly under-predicted the observation at 1.592σ. However, the intentionally conservative second calculation, $F_{peak_{Design}}$, which is based on the maximum drag coefficient estimate, over-predicted the load at -3.836σ.

During parachute descent, the spacecraft decelerated from 406.349 m/s to 78.886 m/s, removing 97.5% of the remaining kinetic energy in just 116.8 s. Total time on chute (-0.029σ) and downrange flown (-0.235σ) were very nominal. Parachute areal oscillations were not observed. Likewise, very nominal wrist mode was experienced, leading to (0.964σ) peak attitude rate and (0.216 σ) peak angular acceleration, as shown in Table 1.

HEATSHIELD JETTISON

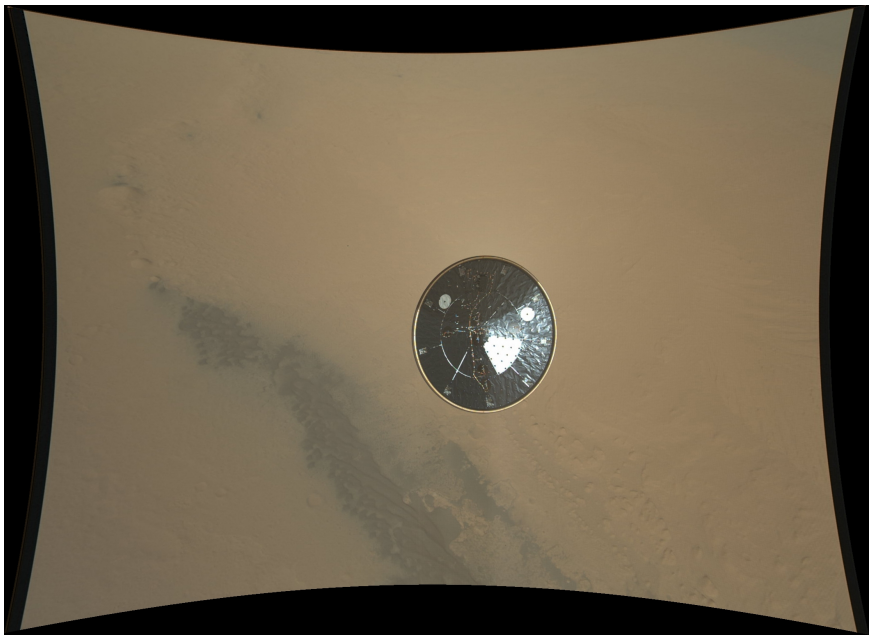

Figure 6: Full-resolution color Mars Descent Imager instrument (MARDI) image of the heatshield obtained about 3 seconds after heatshield jettison. Range to the heatshield is approximately 16 meters. Image Credit: NASA/JPL-Caltech/MSSS.

Following parachute deploy, the vehicle quickly decelerated to subsonic conditions and the spacecraft initiated a series critical events required to be performed in preparation for powered descent. The first of these critical events is the jettison of the heatshield. Constraints were placed on this event to satisfy two requirements: positive separation from the flight system to prevent re-contact and sufficient separation distance prior to initiating TDS measurements to ensure that the heatshield could not simultaneously block more than one beam. Attitude rates at heatshield separation were also limited to prevent near-term recontact.

Heatshield jettison occurred at $t = 7818.875\ s$, $R_{down} = 0.758\ km$, and $R_{cross} = 0.194\ km$. Additional flight conditions were reconstructed by Cruz et al.[7] Flight conditions at heatshield jettison were very nominal: Mach number (0.489σ), dynamic pressure (0.042σ), altitude (0.177σ), and flight path angle (-0.168σ).

Due to the large ballistic coefficient mis-match between the heatshield and rest of the flight system, mid- to long-term recontact was considered to be a very low risk event. However, the POST2 simulation was used to assess the separation distance achieved within the first five seconds after jettison to verify the second heatshield requirement. Push-off springs were sized in impart approximately 2 m/s of push-off velocity to help achieve at least 15 m separation during this time. These springs were not modeled in the simulation, however, to add additional conservatism to the predicted separation rates.

The validity of the heatshield separation predictions may be assessed by two independent sources of flight data. First, images taken by the Mars Descent Imager (MARDI) during EDL (such as Figure 6), were used to estimate the separation distance from the flight system to the heat-shield by calculating the percentage of pixels occupied by the heatshield. Second, the Terminal Descent Sensor (TDS) fortuitously measured the range and range rate to the heatshield at approximately 29 s after heatshield separation. Utilizing predictions from the OD230 POST2 Monte Carlo, the 1, 10, 50, 90 and 99 %-tile bounds of separation distance were overlaid on the MARDI raw, MARDI smoothed, and TDS data, as shown in the left plot of Figure 7.

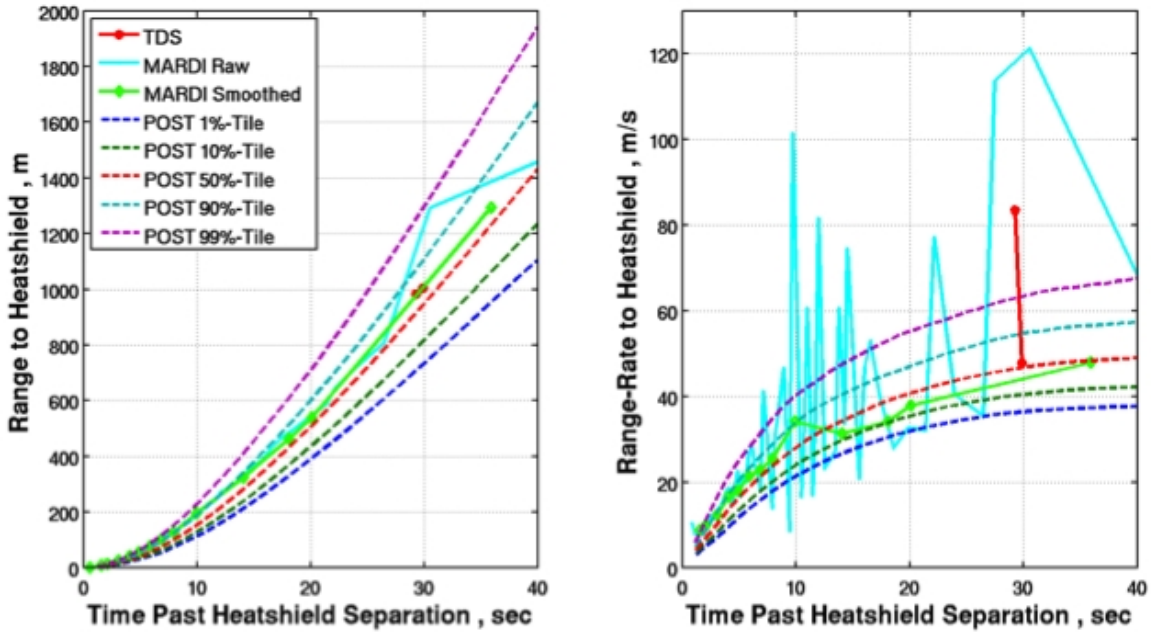

Figure 7: Needs caption.

Figure 7 shows the POST2 separation profile predicted a shorter initial separation distance relative to the flight data, as intended to stress the short-term separation analysis. Additionally, the simulation did well at predicting the long-term separation profile. The range-rate POST2 Monte Carlo bounds, MARDI raw, MARDI smoothed and TDS data are plotted in the right plot of Figure 7. Results show the push-off rate was near the POST 99 %-tile predicted results, due to the lack of modeling the push-off springs. However, the simulation predictions en-compassed the MARDI smoothed data in the long-term separation rate profile. The MARDI raw reconstructed range-rates are very noisy due to finite differencing the quantized pixel counts at large distances.

NAV ALTITUDE SOLUTION

After the parachute had been safely deployed, the vehicle had slowed to subsonic speeds, and the heatshield had been jettisoned, the next critical event was for the Terminal Descent System (TDS) to acquire the ground. It was necessary for the TDS to accurately measure the vehicle's altitude and velocity, relative to the surface of Mars, before proceeding with powered descent. GN&C Mode 20, "TDS NAV INIT", began when the vehicle was ready to process TDS data (approximately 5 seconds after heatshield separation) and ended when the navigation filter converged on an altitude solution. At that point, the mode changed to Mode 21, "MLE PRIMING LOGIC ENABLED".

NAV solution occurred at $t = 837.125\ s$, $R_{down} = -0.741\ km$, $R_{cross} = 0.210$, and altitude $h_{AGL} = 8.355\ km$. The observed times in GN&C modes 20 and 21 were 13.125 s (-1.45σ) and 62.5 s (2.25σ), respectively. When considered together, however, the combined time in both Mode 20 and Mode 21 was 75.625 s, which is very close to the predicted mean and just 0.105σ. This indicates that the total time on parachute was very nominal. The shorter than nominal time in Mode 20, followed by a longer than nominal time in Mode 21, is due to TDS performance exceeding the conservative estimates of the level-1 TDS model. However, the longer time in Mode 21 was correctly predicted by a more detailed physics-based model of the TDS, known as Sulcata.[?]

POWERED DESCENT

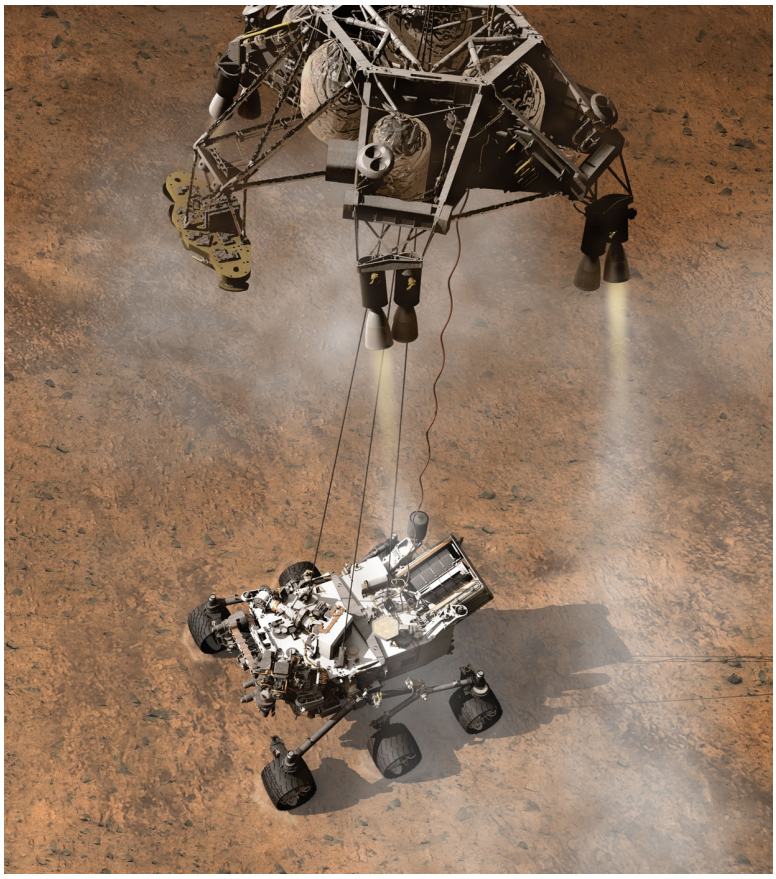

Figure 8: Artist's concept of the novel Sky Crane system used to land *Curiosity*. Image Credit: NASA/JPL-Caltech.

The Powered Descent Segment begins with Backshell Separation and consists of four sub-segments, separated by altitude-velocity waypoints: Powered Approach, Constant Velocity Accordion, Constant Deceleration, and Sky Crane. During powered approach, the PDV followed a computed polynomial trajectory that diverted the PDV 300 m perpendicular to the flight system motion, nulled the horizontal velocity, and achieved a 32 m/s constant vertical velocity. During the constant velocity accordion, the flight system was able to compensate for up to 100 m of terrain variation. During Constant Deceleration, the descent rate was slowed from 32 m/s to 0.75 m/s. Finally, during Sky Crane, the rover was lowered on the BUD, and the rover mobility was deployed in anticipation of touchdown.

Backshell Separation occurred at $t = 915.921875\ s$, $R_{down} = -2.089\ km$, and $R_{cross} = 0.332\ km$. Additional flight conditions were reconstructed by Cruz et al.[7] These constructed flight conditions were very nominal: Mach number (0.883σ), dynamic pressure (0.393σ), altitude (0.053σ), and flight path angle (-0.348σ). An important propulsion system requirement was to ensure that at least 8 s of MLE priming time were observed before firing PV-6. The as-flown time of 17.3 s, or -0.198σ, more than doubled this requirement.

Powered Descent proceeded nominally through all of the designed altitude-velocity waypoints. As shown in Table 1, the constant velocity accordion, which consumed only 5.5 m of the available 100 m accordion, was 0.619σ relative to simulation predictions. Likewise, the 5.13 m touchdown accordion, which consumed less than 1 m of the available 5 m, was 0.461σ. Additionally, the 5.3 s rover deployment time (-0.412σ) was

only 0.09 s shorter than the mean time predicted by the BUD model.

However, the third, and most serious anomaly during EDL was observed in the last few seconds of powered flight. The cause of the anomaly was determined to be the result of a 450 μg error in estimating the local gravitational acceleration at the landing site.[15] This error produced a 2.58σ long time in GN&C Mode 35, "PD READY FOR TOUCHDOWN", and a related 2.563σ long "RVR MOB SEP" timeline anchor chain margin as a result of a 0.1 m/s error in propagating the vertical velocity. This situation arises when four of the six TDS beams are secured following rover separation. The end result was a touchdown velocity that was 3.772σ horizontal and -3.836σ vertical. In-flight, the sense of the error resulted in a softer than expected touchdown. However, had the local gravity been under-estimated, instead of over-estimated, the maximum touchdown velocity of 0.85 m/s could have been exceeded. This EDL sensitivity to small errors in the gravity field may be designed-out of future missions by ensuring that three or more TDS beams are providing valid measurements all the way to touchdown.

LANDING

Curiosity landed safely on Mars, August 5, 2012, at 22:32 PDT (Earth Received Time). Immediately following landing, one of the first reconstruction tasks facing the EDL team was to locate the landed position of the rover. A Landing Location Working Group (LLWG) was organized for just this purpose. The group's first estimate (4.59 ^oS, 137.44 ^oE), provided within minutes of the landing, was accurate to within 104.6 m. This estimate (shown in Figure 9) combined expected navigation errors from the POST2 simulation results with the estimated landing position reported by the onboard navigation system.[11] The predicted 99%-tile footprint for the OD229 navigation solution was 18.59 x 6.37 km. *Curiosity*'s actual landing site (4.5895 ^oS, 137.4417 ^oE) was only 2.385 km from the target, which represents a 0.747σ or 23.75%-tile landing, as determined by using the Cholesky decomposition of the covariance matrix. This method is similar to the process used in constructing the landing footprint ellipses for plots such as Figure 9. When comparing the miss-distance without regard to azimuth, the quantile is 1.146σ, as shown in Table 1.

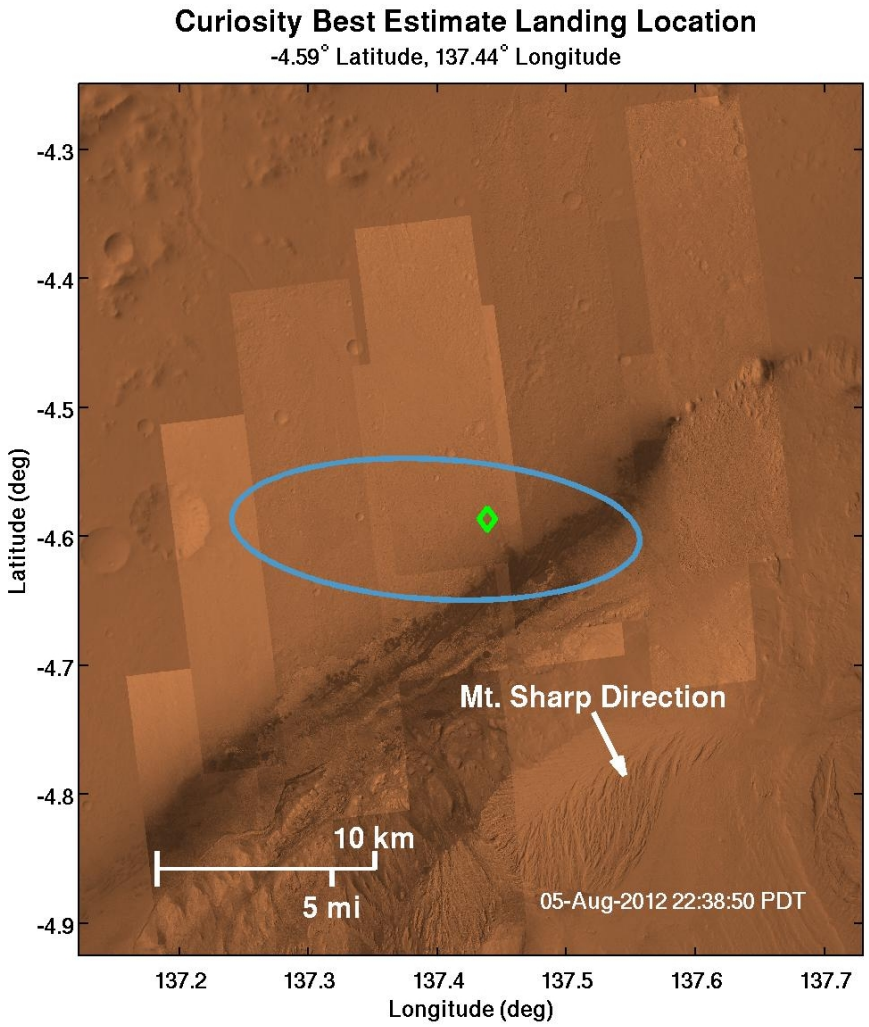

Figure 9: Initial landing location estimate, made within minutes of landing. This estimate combined expected navigation errors from the POST2 simulation results with the estimated landing position reported by the onboard navigation system.

SCORE CARD

Table 1 compares reconstructed flight parameters to pre-flight simulation predictions. The 1%-tile, mean, and 99%-tile statistics from the OD229 Monte Carlo are compared to as-flown values, compiled from multiple sources. In each case, the Gaussian quantile of the as-flown value is measured, relative to the simulation results. This measurement is expressed as a number of standard deviations (e.g. 3σ) and serves as the primary basis for measuring the quality and conservatism of the pre-flight predictions. Values within approximately +/-1.5σ indicate good agreement, while values outside of +/-3σ indicate a significant disagreement between actual and simulated results. For one-sided distributions, the as-flown value is compared to standard Rayleigh quantiles, rather than Gaussian. Where this was done, the calculated quantile is denoted with a superscripted asterisk.

Table 1: EDL Scorecard.

Score Card Item		Design Requirement		EDL Simulation OD229 Monte Carlo Results			Flight Reconstruction	
Description	**Units**	**<=>**	**Limit**	**1%**	**Mean**	**99%**	**Value$^{Ref.}$**	**Quantile**
Telecommunications.								
MRO UHF Loss of Signal	$E+mm:ss$			12 : 50	12 : 57	13 : 03	13 : 08[?]	3.557σ
MRO UHF Signal Acquisition	$E-mm:ss$			07 : 36	07 : 48	08 : 20	08 : 07[?]	1.494σ
ODY UHF Signal Acquisition	$E+mm:ss$			02 : 44	02 : 46	02 : 47	03 : 42[?]	3.836σ
ODY UHF Loss of Signal	$E+mm:ss$			12 : 29	14 : 02	15 : 10	13 : 07[?]	-0.973σ
Atmospheric Entry.								
Peak Entry Deceleration	Earth $g's$	$<$	15	12.260	12.712	13.248	12.609[1]	-0.471σ
Peak Entry Lateral Loads	Earth $g's$	$<$	0.65	0.355	0.447	0.548	0.492	1.060σ
Peak Parachute Decleration	Earth $g's$			5.340	6.694	8.370	6.068[1]	-0.806σ
Peak Pressure	atm	$<$	0.36	0.301	0.315	0.331	0.305[?]	-1.658σ
Prebank Error	deg	$<$	30	0.055	3.010	8.553	8.595	3.050σ*
Downrage at HDA	km			76.314	81.482	86.361	83.242[?]	0.706σ
Downrage at SUFR	km			7.862	14.119	20.320	12.819[?]	-0.473σ
Downrange at PD	km			1.103	7.332	13.538	4.966[?]	-0.889σ
Downrange at TD	km			-7.475	-0.124	7.076	-2.329[?]	-0.699σ
Entry Control.								
Warm-up to TTE Attitude Error (x)	deg			2.028	2.902	5.608	2.232[14]	0.401σ*
Warm-up to TTE Attitude Error (y)	deg			2.014	2.926	5.543	2.019[14]	0.149σ*
Warm-up to TTE Attitude Error (z)	deg			1.620	2.698	5.573	2.297[14]	0.642σ*
Warm-up to TTE Rate Error (x)	deg/s			0.436	1.397	2.762	0.662[14]	0.323σ*
Warm-up to TTE Rate Error (y)	deg/s			0.571	1.546	3.061	0.554[14]	0.125σ*
Warm-up to TTE Rate Error (z)	deg/s			0.360	1.248	2.732	0.584[14]	0.383σ*
Exo-atmospheric Attitude Error (x)	deg			1.973	2.695	4.920	2.031[14]	0.522σ*
Exo-atmospheric Attitude Error (y)	deg			4.880	5.003	5.246	4.974[14]	1.109σ*
Exo-atmospheric Attitude Error (z)	deg			1.968	3.308	4.980	3.377[14]	1.321σ*
Exo-atmospheric Rate Error (x)	deg/s			0.242	1.142	2.652	0.431[14]	0.359σ*
Exo-atmospheric Rate Error (y)	deg/s			0.746	1.281	2.660	1.354[14]	1.509σ*
Exo-atmospheric Rate Error (z)	deg/s			0.156	0.691	1.910	0.534[14]	1.067σ*
Range Control Attitude Error (x)	deg			0.947	2.020	3.966	0.877[14]	0.092σ*
Range Control Attitude Error (y)	deg			1.148	2.132	3.783	1.637[14]	0.638σ*
Range Control Attitude Error (z)	deg			6.587	9.062	20.068	5.782[14]	0.025σ*
Range Control Rate Error (x)	deg/s			1.810	3.076	5.128	2.059[14]	0.249σ*
Range Control Rate Error (y)	deg/s			2.410	3.891	6.698	2.890[14]	0.626σ*
Range Control Rate Error (z)	deg/s			2.414	4.231	13.545	3.243[14]	0.652σ*
Hdg. Align. Attitude Error (x)	deg			1.792	3.248	5.757	1.822[14]	0.146σ*

* Note: One-sided distributions are compared to standard Rayleigh quantiles.

Table 1 – *Continued on the next page*

Table 1 – *Continued from the previous page*

Score Card Item		Design Requirement		EDL Simulation OD229 Monte Carlo Results			Flight Reconstruction	
Description	**Units**	**<=>**	**Limit**	**1%**	**Mean**	**99%**	**Value**$^{Ref.}$	**Quantile**
Hdg. Align. Attitude Error (y)	deg			2.075	3.717	6.625	3.209[14]	0.920σ*
Hdg. Align. Attitude Error (z)	deg			5.171	8.281	11.888	7.355[14]	0.865σ*
Hdg. Align. Rate Error (x)	deg/s			1.389	2.694	5.274	1.166[14]	0.089σ*
Hdg. Align. Rate Error (y)	deg/s			2.244	3.000	5.992	2.352[14]	0.446σ*
Hdg. Align. Rate Error (z)	deg/s			1.947	4.308	7.534	2.663[14]	0.438σ*
SUFR Attitude Error (x)	deg			1.970	3.953	7.248	4.594[14]	1.643σ*
SUFR Attitude Error (y)	deg			3.149	6.401	10.913	8.108[14]	1.867σ*
SUFR Attitude Error (z)	deg			3.732	5.331	6.203	5.908[14]	2.178σ*
SUFR Rate Error (x)	deg/s			2.272	2.816	3.325	2.753[14]	0.975σ*
SUFR Rate Error (y)	deg/s			2.354	2.844	3.772	2.690[14]	0.895σ*
SUFR Rate Error (z)	deg/s			0.484	1.785	3.796	3.618[14]	2.787σ*
RCS Thruster 1 Firings				368	471	624	368[14]	0.140σ*
RCS Thruster 2 Firings				163	250	322	255[14]	1.189σ*
RCS Thruster 3 Firings				275	391	587	309[14]	0.427σ*
RCS Thruster 4 Firings				119	207	274	190[14]	0.819σ*
RCS Thruster 5 Firings				321	450	671	376[14]	0.628σ*
RCS Thruster 6 Firings				150	248	333	249[14]	1.112σ*
RCS Thruster 7 Firings				309	412	566	319[14]	0.215σ*
RCS Thruster 8 Firings				126	211	289	192[14]	0.782σ*
Footprints.								
Landing Accuracy	km	$<$	12.5	0.289	2.834	8.110	2.385[11]	1.146σ*
Parachute Deploy Conditions.								
Mach No. at Parachute Deploy		$<$	2.3	1.549	1.695	1.868	1.75[7]	0.749σ
Dynamic Pressure At PD	Pa	$<$	700	431.7	494.9	564.8	493.6[7]	-0.019σ
Total AoA at Parachute Deploy	deg	$<$	12	0.22	1.92	4.55	3.52[7]	2.341σ*
Altitude at Parachute Deploy	km			4.7768	7.3881	10.0784	7.5429[7]	0.144σ
Flight Path Angle at PD	deg			-23.3853	-20.8256	-18.1255	-22.4[7]	-1.345σ
Parachute Descent.								
Areal Oscillation Exposure	s			0.53	1.51	2.90	1.75[7]	0.532σ
Parachute Peak Inflation Load (Model)	1000 lb_f	$<$	65	22.81	29.06	36.79	34.58[7]	1.592σ
Parachute Peak Inflation Load (Design)	1000 lb_f	$<$	65	43.09	49.85	56.94	34.58[7]	-3.836σ
Peak Angular Acceleration	rad/s^2	$<$	37.1	7.17	11.10	19.58	10.88[1]	0.216σ
Peak Attitude Rate	deg/s	$<$	120	23.78	53.39	103.40	69.39[1]	0.964σ
Heatshield Jettison Conditions.								
Mach No. at HSS		$<$	0.8	0.5002	0.59562	0.70486	0.618[7]	0.489σ
Dynamic Pressure At HSS	Pa			55.4904	74.6075	94.8956	74.9[7]	0.042σ
Altitude at HSS	km			2.6167	5.1811	7.9435	5.3598[7]	0.177σ
Flight Path Angle at HSS	deg			-47.5908	-35.4401	-20.7682	-37[7]	-0.168σ

* Note: One-sided distributions are compared to standard Rayleigh quantiles.

Table 1 – *Continued on the next page*

Table 1 – *Continued from the previous page*

Score Card Item		Design Requirement		EDL Simulation OD229 Monte Carlo Results			Flight Reconstruction	
Description	**Units**	**<=>**	**Limit**	**1%**	**Mean**	**99%**	**Value**$^{Ref.}$	**Quantile**
Backshell Separation.								
Mach No. at BSS				0.29145	0.31299	0.33327	0.324[7]	0.883σ
Dynamic Pressure At BSS	Pa			35.5835	40.9859	46.2941	42.2[7]	0.393σ
Altitude at BSS	km			-2.9069	-2.8338	-2.7566	-2.8328[7]	0.053σ
Flight Path Angle at BSS	deg			-89.3514	-83.7558	-73.0157	-85.5[7]	-0.348σ
Powered Descent.								
Backshell Sep. Altitude	m			1597	1663	1726	1674[?]	0.390σ
Const. Decel. Start Alt.	m			139.70	141.64	143.42	142 .7[?]	1.435σ
Const. Vel. Accordian Start Alt.	m			221.37	242.47	263.38	248[?]	0.688σ
"Fuel Use, Powered Flight"	kg			279.07	287.72	297.72	270[?]	-3.836σ
Powered Descent Duration	s			50.17	53.79	58.06	55.6[?]	1.095σ
Priming time (PV-5 to PV-6)	s	$>$	8	13.9525	17.9057	23.9525	17.3[?]	-0.198σ
Rover Deployment Duration	s			4.98	5.39	5.80	5.3[?]	-0.412σ
Rover Separation Altitude	m			19.49	20.68	21.85	21.5[?]	1.409σ
TD Horizontal Velocity	m/s	$<$	0.1	0.00	0.04	0.09	0.12[?]	3.772σ
TD Vertical Velocity	m/s	$<$	0.85	0.67	0.75	0.82	0.6[?]	-3.836σ
Vel. at Rover Separation	m/s			0.66	0.75	0.85	0.77[?]	0.357σ
Const. Vel. Accordion Flown	m			81.1996	100.8295	120.5427	105.5[?]	0.619σ
Touchdown Accordian Flown	m			4.0561	4.9587	5.8109	5.13[?]	0.461σ
Velocity at Backshell Sep.	m/s			59.24	77.42	95.35	78.6[?]	0.132σ
Altitude AGL at TDS Nav Init	km	$>$	3	5.712	6.815	7.637	8.346[?]	3.836σ
Time in GN&C Mode.								
Time in GN&C Mode 4	s			20.500	20.500	20.500	20.500[1]	-3.836σ
Time in GN&C Mode 5	s			5.500	6.238	7.000	6.500[1]	1.021σ
Time in GN&C Mode 6	s			9.000	22.295	38.125	23.625[1]	0.159σ
Time in GN&C Mode 7	s			475.250	491.092	504.500	489.375[1]	-0.178σ
Time in GN&C Mode 8	s			46.375	47.177	48.000	45.875[1]	-3.836σ
Time in GN&C Mode 9	s			0.250	1.674	3.000	3.000[1]	2.509σ
Time in GN&C Mode 10	s			52.375	56.360	64.061	54.250[1]	-1.197σ
Time in GN&C Mode 11	s			22.250	31.093	34.375	32.500[1]	0.641σ
Time in GN&C Mode 12	s			1.250	5.206	9.750	5.125[1]	0.034σ
Time in GN&C Mode 13	s			83.375	94.051	104.125	99.125[1]	1.120σ
Time in GN&C Mode 14	s			13.000	13.693	14.000	14.000[1]	0.814σ
Time in GN&C Mode 15	s			1.250	2.848	4.750	5.250[1]	2.931σ
Time in GN&C Mode 16	s			10.016	10.016	10.016	10.016[1]	-3.836σ
Time in GN&C Mode 17	s			6.484	11.349	16.170	9.734[1]	-0.806σ
Time in GN&C Mode 18	s			3.125	3.125	3.125	3.016[1]	-3.836σ
Time in GN&C Mode 19	s			2.000	2.000	2.000	2.109[1]	3.836σ

* Note: One-sided distributions are compared to standard Rayleigh quantiles.

Table 1 – *Continued on the next page*

Table 1 – *Continued from the previous page*

Score Card Item		Design Requirement		EDL Simulation OD229 Monte Carlo Results			Flight Reconstruction	
Description	**Units**	**<=>**	**Limit**	**1%**	**Mean**	**99%**	**Value$^{Ref.}$**	**Quantile**
Time in GN&C Mode 20	s			8.125	29.385	61.125	13.125[1]	-1.445σ
Time in GN&C Mode 21	s	$>$	5	29.750	45.602	63.250	62.500[1]	2.251σ
Time in GN&C Mode 22	s			11.750	15.703	21.750	14.875[1]	-0.264σ
Time in GN&C Mode 23	s			1.423	1.423	1.423	1.422[1]	-3.836σ
Time in GN&C Mode 24	s			0.985	0.985	0.985	0.969[1]	-3.836σ
Time in GN&C Mode 25	s			0.203	0.203	0.203	0.219[1]	3.836σ
Time in GN&C Mode 26	s			0.033	0.173	0.423	0.156[1]	-0.027σ
Time in GN&C Mode 27	s			0.375	1.030	1.765	1.109[1]	0.285σ
Time in GN&C Mode 28	s			18.795	21.864	25.717	21.656[1]	-0.076σ
Time in GN&C Mode 29	s			2.530	3.148	3.766	3.047[1]	-0.455σ
Time in GN&C Mode 30	s			6.532	7.255	7.625	7.281[1]	0.274σ
Time in GN&C Mode 33	s			2.530	2.531	0.268	2.531[1]	0.301σ
Time in GN&C Mode 34	s			8.968	8.969	8.970	8.969[1]	0.671σ
Time in GN&C Mode 35	s			6.008	7.596	9.422	9.656[1]	2.580σ
Time in GN&C Mode 36	s			0.593	0.594	0.595	0.594[1]	0.656σ
Time in GN&C Mode 37	s			0.202	0.203	0.203	0.203[1]	-1.151σ
Timeline Engine Chain Margin.								
TZERO NAV GNC START Margin	s	$>$	0	35.625	49.033	64.875	50.625	0.169σ
ENTRY CG CBM Margin	s	$>$	0	294.625	310.467	323.875	308.828	-0.178σ
ENTRY GNC Margin	s	$>$	0	128.000	128.000	128.000	128.000	0.000σ
TDS PWR TDS START Margin	s	$>$	0	87.689	97.686	108.500	101.922	0.901σ
SUFR Margin	s	$>$	0	3.500	5.040	6.875	7.750	3.200σ
PD Margin	s	$>$	0	3.063	7.927	12.749	6.313	-0.870σ
HSS Margin	s	$>$	0	0.719	0.719	0.719	0.719	0.000σ
HSS RCS CNTRL Margin	s	$>$	0	0.875	0.875	0.875	0.875	0.000σ
HSS START TDS NAV INIT Margin	s	$>$	0	39.969	73.580	118.094	74.219	0.100σ
PRIM MLE Margin	s	$>$	0	11.594	15.547	21.594	14.719	-0.335σ
BSS Margin	s	$>$	0	0.688	0.688	0.688	0.688	0.000σ
BSS MLE Warmup Margin	s	$>$	0	19.922	22.824	26.648	22.578	-0.100σ
SKYCRANE Margin	s	$>$	0	1.734	1.734	1.734	1.734	0.000σ
RVR MOB SEP Margin	s	$>$	0	15.602	17.190	19.016	19.250	2.563σ

* Note: One-sided distributions are compared to standard Rayleigh quantiles. End – **Table 1**.

CONCLUSIONS

The POST2 MSL end-to-end EDL simulation played a critical role in the successful landing of the *Curiosity* rover on Mars, August 5, 2012. Simulation predictions were used throughout the project lifecycle: to inform EDL design choices, to compare and certify candidate landing sites, to verify EDL system performance, to select GN&C parameters, and to evaluate TCM and EPU operational decisions. Considering the importance of these activities, it is evident that the EDL simulation must accurately, yet conservatively, predict EDL system behavior. It is desired, therefore, to evaluate the effectiveness of the EDL simulation by comparing flight data to pre-entry simulation predictions. This paper provided a quick-look at this comparison, using data available shortly after landing. The following specific observations were discussed:

1. The predicted 99%-tile footprint for the OD229 navigation solution was 18.59 x 6.37 km. *Curiosity*'s actual landing site (4.5895 ^oS, 137.4417 ^oE) was only 2.385 km from the target, which represents a 0.74725σ or 23.747%-tile landing.

2. All Timeline Engine timepoints occurred within 6.9089 s of their predicted mean times. However, the cumulative time in several of the GN&C Mode Commander states exceeded +/- 1.5σ of the simulation results. These modes were investigated in more detail.

3. A very short -3.836σ time in GN&C Mode 8, "WAIT FOR GUIDANCE START", was observed due to higher than expected deceleration at altitudes above 50 km. The immediate effect was for the guidance to command an initial bank angle 8.594817 deg away from the expected pre-bank angle. There were no lasting effects, however, as the vehicle recovered rapidly from this anomaly.

4. Low supersonic deceleration during the SUFR maneuver resulted in a combined 3.23σ time in GN&C Modes 14 and 15. During this time it is estimated that the vehicle lost approximately 340 m of altitude, which was of little consequence due the ample altitude margin at Gale crater. Additional investigation into this anomaly is warranted, however, to better understand the expected aerodynamic performance in this flight regime.

5. TDS maximum range capability exceeded the conservative estimates of the level-1 TDS model. This lead to -1.45σ and 2.25σ times in GN&C Modes 20 and 21. However, the longer time in Mode 21 was correctly predicted by a more detailed physics-based model of the TDS, known as Sulcata.

6. A 2.58σ long time in GN&C Mode 35, "PD READY FOR TOUCHDOWN", was determined to be due to an error in estimating the local gravitational acceleration at the landing site. In-flight, this error resulted in a softer than expected touchdown. However, had the local gravity been under-estimated, instead of over-estimated, a maximum touchdown velocity of 0.85 m/s could have been exceeded. This EDL sensitivity to small errors in the gravity field may be designed-out of future missions by ensuring that three or more TDS beams are providing valid measurements all the way to touchdown.

7. As-flown values for peak deceleration during entry (12.609 $Earth\ g's$) and on parachute (6.068 $Earth\ g's$) were within -0.471σ and -0.806σ of simulation predictions, respectively. Indicating very good entry and parachute model performance.

8. The peak attitude rate (69.39 deg/s) and angular acceleration (10.881 rad/s^2) watermarks were predicted well by the simulation at 0.964σ and 0.216σ, respectively. These indicated that the vehicle experienced very nominal wrist mode oscillations while on parachute. This is extremely good agreement, given the difficulty and complexity of modeling parachute dynamics in an EDL simulation.

NOMENCLATURE

σ	Standard deviation
ATLO	Assembly, Test, and Launch Operations
BUD	Bridle, Umbilical, and DRL
DGB	Disk-Gap-Band parachute
DoF	Degrees of Freedom
DRL	Descent Rate Limiter
DSN	Deep Space Network
EBMD	Entry Balance Mass Device
EDL	Entry, Descent, and Landing
EPU	EDL Parameter Update
EVR	EVent Report real-time telemetry
GN&C	Guidance, Navigation, and Control
IMU	Inertial Measurement Unit
LLWG	Landing Location Working Group
MER	Mars Exploration Rover mission
MSL	Mars Science Laboratory mission
OD	Orbit Determination
POST2	Program to Optimize Simulated Trajectories II
RTI	Run Time Interrupt, 8 Hz
sRTI	Sub-RTI, 64 Hz
SUFR	Straighten-Up and Fly Right
TCM	Trajectory Correction Maneuver
TDS	Terminal Descent Sensor – RADAR
TPS	Thermal Protection System
TZERO	EDL GN&C start time, $t = 0s$

ACKNOWLEDGMENTS

The development of a simulation as complex as this one is not possible without the contributions of many people. Each of the model developers has made a significant contribution to the MSL project and the EDL community. The authors would like to thank the many members of the MSL EDL team who contributed to the successful landing of the *Curiosity* rover. It was a privilege and an honor to have worked with such a capable and talented team.

REFERENCES

[1] D. Way, "Preliminary Assessment of the Mars Science Laboratory Entry, Descent, and Landing Simulation," IEEE-2013-2755, *IEEE Aerospace Conference*, Big Sky, MT, Mar. 2013.

[2] A. Steltzner, D. Kipp, A. Chen, P. D. Burkhart, C. Guernsey, G. Mendeck, R. Mitcheltree, R. Powell, T. Rivellini, A. M. San Martin, and D. Way, "Mars Science Laboratory Entry, Descent, and Landing System," IEEE-2006-1497, *IEEE Aerospace Conference*, Big Sky, MT, Mar. 2006.

[3] R. Prakash, P. D. Burkhart, A. Chen, K. Comeaux, C. Guernsey, D. Kipp, L. Lorenzoni, G. Mendeck, R. Powell, T. Rivellini, A. M. San Martin, S. Sell, A. Steltzner, and D. Way, "Mars Science Laboratory Entry, Descent, and Landing System Overview," IEEE-2007-1531, *IEEE Aerospace Conference*, Big Sky, MT, Mar. 2008.

[4] R. D. Braun, R. W. Powell, W. C. Engelund, P. A. Gnoffo, J. K. Weilmunster, and R. A. Mitcheltree, "Mars Pathfinder Six-Degree-of-Freedom Entry Analysis," *Journal of Spacecraft and Rockets*, Vol. 32, No. 6, pp. 993–1000, Nov.–Dec. 1995.

[5] P. N. Desai, M. Schoenenberger, and F. M. Cheatwood, "Mars Exploration Rover Six-Degree-of-Freedom Entry Trajectory Analysis," *Journal of Spacecraft and Rockets*, Vol. 43, No. 5, pp. 1019–1025, Sep.–Oct. 2006.

[6] J. L. Prince, P. N. Desai, E. M. Queen, and M. R. Grover, "Mars Phoenix Entry, Descent, and Landing Simulation Design and Modeling Analysis," AIAA-2008-7507, *AIAA/AAS Astrodynamics Specialist Conference and Exhibit*, Honolulu, HI, Aug. 2008.

[7] J. R. Cruz, D. W. Way, J. D. Shidner, J. L. Davis, D. S. Adams, and D. M. Kipp, "Reconstruction of the Mars Science Laboratory Parachute Performance and Comparison to the Descent Simulation," AIAA-2013-XXXX, *22nd AIAA Aerodynamic Decelerator Systems Technology Conference* , Daytona Beach, FL, Mar. 2013.

[8] P. N. Desai, J. L. Prince, E. M. Queen, J. R. Cruz, and M. R. Grover, "Entry, Descent, and Landing Performance of the Mars Phoenix Lander," AIAA-2008-7346, *AIAA Guidance, Navigation, and Control Conference*, Honolulu, HI, Aug. 2008.

[9] B. Raiszadeh and E. M. Queen, "Mars Exploration Rover Terminal Descent Mission Modeling and Simulation," AAS 04-271, *AAS/AIAA Space Flight Mechanics Meeting*, Maui, HI, Feb. 2004.

[10] E. M. Queen, J. L. Prince, and P. N. Desai, "Multi-Body Modeling and Simulation for the Mars Phoenix Lander Entry, Descent and Landing," AIAA-2008-7347, *AIAA Guidance, Navigation, and Control Conference*, Honolulu, HI, Aug. 2008.

[11] J. L. Davis, J. D. Shidner, and D. W. Way, "Mars Science Laboratory Post-Landing Location Estimation Using POST2 Trajectory Ssimulation," AAS 13-313, *AAS/AIAA 23rd Space Flight Mechanics Meeting*, Kauai, HI, Feb. 2013.

[12] A. Steltzner, "Mars Science Laboratory Entry, Descent and Landing System Overview," AAS 13-236, *AAS/AIAA 23rd Space Flight Mechanics Meeting*, Kauai, HI, Feb. 2013.

[13] T. Martin-Mur, "Mars Science Laboratory Interplanetary Navigation Performance," AAS 13-232, *AAS/AIAA 23rd Space Flight Mechanics Meeting*, Kauai, HI, Feb. 2013.

[14] P. Brugarolis, A. M. San Martin, and E. Wong, "The MSL Entry Controller," AAS 13-235, *AAS/AIAA 23rd Space Flight Mechanics Meeting*, Kauai, HI, Feb. 2013.

[15] F. Serricchio, A. M. San Martin, and E. Wong, "The MSL Navigation Filter," AAS 13-418, *AAS/AIAA 23rd Space Flight Mechanics Meeting*, Kauai, HI, Feb. 2013.

[16] G. Mendeck and L. McGrew, "Post-Flight EDL Entry Guidance Performance of the 2011 Mars Science Laboratory Mission," AAS 13-419, *AAS/AIAA 23rd Space Flight Mechanics Meeting*, Kauai, HI, Feb. 2013.

[17] A. Chen, "Entry System Design and Performance Summary for the Mars Science Laboratory Mission," AAS 13-422, *AAS/AIAA 23rd Space Flight Mechanics Meeting*, Kauai, HI, Feb. 2013.

[18] A. Chen, "Approach and Entry, Descent, and Landing Operations for the Mars Science Laboratory Mission," AAS 13-425, *AAS/AIAA 23rd Space Flight Mechanics Meeting*, Kauai, HI, Feb. 2013.

[19] B. Schratz, A. Chen, F. Abilleira, and J. Shidner, "Telecom Performance and Mission Design during the Entry Descent and Landing of the Mars Science Laboratory," AAS 13-312, *AAS/AIAA 23rd Space Flight Mechanics Meeting*, Kauai, HI, Feb. 2013.

[20] M. Schoenenberger, J. Van Norman, A. Dyakonov, C. Karlgaard, D. Way, and P. Kutty, "Assessment of the Reconstructed Aerodynamics of the Mars Science Laboratory Entry Vehicle," AAS 13-306, *AAS/AIAA 23rd Space Flight Mechanics Meeting*, Kauai, HI, Feb. 2013.

[21] F. Auger and P. Flandrin, "Improving the readability of time-frequency and time-scale representations by the reassignment method," *IEEE Transactions on Signal Processing*, Vol. 43, No. 5, pp. 1068–1089, May. 1995.